UCLA
UCLA Previously Published Works

Title
Theta Oscillations in the Human Medial Temporal Lobe during Real-World Ambulatory Movement

Permalink

Journal

ISSN

Authors
Aghajan, Zahra M
Schuette, Peter
Fields, Tony A
et al.

Publication Date

DOI

Peer reviewed

Theta Oscillations in the Human Medial Temporal Lobe during Real World Ambulatory Movement

Zahra M. Aghajan[1], **Peter Schuette**[1], **Tony Fields**[2], **Michelle Tran**[3], **Sameed Siddiqui**[1], **Nick Hasulak**[4], **Thomas K. Tcheng**[4], **Dawn Eliashiv**[2], **Emily A. Mankin**[3], **John Stern**[2], **Itzhak Fried**[1,3,5,6], and **Nanthia Suthana**[1,3,7,*]

[1]Department of Psychiatry and Biobehavioral Sciences, Semel Institute for Neuroscience and Human Behavior, University of California Los Angeles, Los Angeles, CA 90095, USA

[2]Department of Neurology, University of California Los Angeles, Los Angeles, CA 90095, USA

[3]Department of Neurosurgery, David Geffen School of Medicine, University of California Los Angeles, Los Angeles, CA 90095, USA

[4]NeuroPace, Inc., Mountain View, CA 94043, USA

[5]Functional Neurosurgery Unit, Tel-Aviv Medical Center, Tel-Aviv 64361, Israel

[6]Sackler Faculty of Medicine, Tel-Aviv University, Tel-Aviv 69978, Israel

[7]Department of Psychology, University of California Los Angeles, Los Angeles, CA 90095, USA

Summary

The theta rhythm—a slow (6–12Hz) oscillatory component of the local field potential—plays a critical role in spatial navigation and memory by coordinating the activity of neuronal ensembles within the medial temporal lobe (MTL). Although theta has been extensively studied in freely moving rodents, in humans, its presence has been elusive and primarily investigated in stationary subjects. Here we used a unique clinical opportunity to examine theta within the human MTL during untethered, real world ambulatory movement. We recorded intracranial electroencephalographic activity from participants chronically implanted with the wireless NeuroPace responsive neurostimulator (RNS®), and tracked their motion with sub-millimeter precision. Our data revealed that movement-related theta oscillations indeed exist in humans, such that theta power is significantly higher during movement than immobility. Unlike in rodents, however, theta occurs in short bouts—with average durations of ~400 ms—which are more

---

[*]Corresponding and lead contact: nsuthana@mednet.ucla.edu.

prevalent during fast versus slow movements. In a rare opportunity to study a congenitally blind participant, we found that both the prevalence and duration of theta bouts were increased relative to the sighted participants. These results provide critical support for conserved neurobiological characteristics of theta oscillations during ambulatory spatial navigation while highlighting some fundamental differences across species in these oscillations between humans and rodents.

eTOC

M. Aghajan *et al.* record deep brain activity, during untethered freely moving behavior, from participants chronically implanted with depth electrodes. They demonstrate that 8Hz theta oscillations, the hallmark of spatial navigation in rodents, also occur in humans albeit in shorter bouts that are more prevalent during fast versus slow movements.

Keywords

Medial Temporal Lobe (MTL); human; theta oscillations; navigation; wireless intracranial recordings; Neuropace responsive neurostimulator

Introduction

The crucial role of the medial temporal lobe (MTL) in declarative memory and encoding new experiences is unequivocal based on an abundant body of literature in humans and many mammalian species [1–3]. It is posited that the ongoing rhythmic oscillatory activity in the local field potential (LFP) is critical for the temporal organization of neural assemblies in this region, allowing appropriate modification of synaptic connections. Additionally, various frequency bands are thought to be involved in different brain functions [4,5]. In particular, the 6–12Hz frequency range—commonly referred to as the theta rhythm—has been associated with exploratory behavior [6,7] and REM sleep [8], and different features of this rhythm have been linked to memory performance on various tasks [9–13].

In the rodent hippocampus, theta oscillations (6–12Hz) are most prominent during locomotion—even during tasks with no memory demand, such as running on linear tracks and random foraging—although a lower frequency theta (3–7Hz) has been reported during immobility periods [14]. Theta has also been reported in other species such as cats [15], and in shorter oscillatory bouts in bats [16,17], non-human primates [18,19], and humans [20–22]. There is, thus, an apparent discrepancy in the presence of persistent movement-related theta across species. This issue is confounded by the fact that—due to restrictions imposed by recording techniques—electrophysiological recordings in primates, contrary to those performed in rodents, have typically employed virtual navigation in stationary subjects. Recent rodent hippocampal recordings during virtual navigation have demonstrated significant differences in theta dynamics between virtual and real world navigation, including lower frequencies and a lack of frequency-speed dependence in virtual navigation [23,24]. In light of these studies, resolving whether persistent movement related theta could be a feature of human navigation will require directly probing the intracranial electroencephalogram (iEEG) during natural voluntary human movement. Movement-related theta was observed in walking humans in one recent study [22]. However, due to lack of

motion tracking, this study did not allow for characterization of theta with respect to movement parameters [22]. We therefore conducted an experiment to elucidate the properties of theta oscillations in the MTL of freely moving humans. This was made possible by using a novel chronic implant that allowed for wireless iEEG recording outside of a restrictive hospital setting.

Results

MTL Recordings in Freely Walking Humans Implanted with the RNS® System

Participants were four neurosurgical patients (one congenitally blind), chronically implanted with the FDA approved NeuroPace RNS® System (responsive neurostimulator)(Figure 1A) for treatment of pharmacologically intractable epilepsy. For participant demographics, see Tables S1, 2. For studying ambulatory movement, the RNS® System provides two significant advantages over traditional recording techniques in the hospital setting: motion and muscle artifacts are entirely eliminated (since the implant is fully shielded); subjects are able to freely move around without the limitations imposed by restrictive hospital equipment, related safety protocols, and tethered implanted wires connected to large recording equipment. The RNS® System recorded continuous bipolar iEEG activity from two adjacent electrode contacts (sampling rate: 250Hz; with an analog filter equivalent to a 1st order Butterworth with 3db attenuation at the cutoff frequencies (4–90Hz); for a detailed description see STAR Methods). Participants with MTL electrodes performed a task in which they were instructed to walk along linear and circular paths at slow and fast speeds. A complete trial consisted of the following four movements: a) slow movement in straight lines; b) slow movement in circles; c) fast movement in straight lines; and d) fast movements in circles; the order of these instructions were randomized (Figure 1B, see STAR Methods). Within each trial, after the participants finished one type of movement, they were temporarily immobile until a pre-recorded voice command informed them to begin the next type of motion.

Motion tracking was performed using the OptiTrack system (Natural Point, Inc.), which was capable of recording participants' positional and rotational information (Figure 1C, d, Movie S1). Position information was recorded simultaneously with iEEG data (Figure 2A, Movie S2, 3; see STAR Methods). The locations of electrodes were determined by co-registration of high-resolution post-operative CT images with high-resolution pre-operative magnetic resonance images (MRI) that had been subjected to automated segmentation of MTL subregions to facilitate visualization (Figure 2B, Table S3, see STAR Methods). Although the RNS® System is implanted in potential seizure onset zones, pairs of electrode contacts frequently span up to 10 mm of tissue, thereby leading to some recordings in healthy tissue. In the current study, each participant had at least one contact ipsi-lateral to the seizure onset zone (Table S3). To further account for epileptic tissue in all contact recordings, we eliminated epochs with putative epileptic activity by using a thresholding algorithm similar to methods previously described [25] (see STAR Methods, Figure S1A) and visual inspection, which resulted in discarding 3% of the data per trial (median, [25th, 75th]=3.04, [1.32, 4.62]%, $N_{participants} = 4$, $N_{trials \times channels} = 112$; Figure S1B). Note that the responsive

therapy (stimulation feature) was turned off during the experiments and hence, there was no stimulation artifact in the data (see STAR Methods).

Theta Oscillations during Movement and Immobility Periods

Examination of raw iEEG traces revealed striking theta oscillations, which were readily visible (Figure 2A, Movie S2, 3). We first sought to examine whether these theta oscillations were more prominent during movement than immobility and would thus be considered an analogue of movement-related theta in rodents. To address this, in each trial a multi-taper power spectrum was calculated within each condition, i.e. movement versus immobility, defined as speeds below 10cm/s. We found that theta power was indeed higher during movement, as shown in individual examples (Figure 3A, Figure S2). The theta power index —a normalized measure of power difference between the two conditions—was significantly positive for all participants (Figure 3B; see STAR Methods) and on the population level (median, [25th, 75th]=0.40, [0.30, 0.51], p=4.56×10^{-20}, Wilcoxon signed rank test, n=112). This analysis assumes that individual data points are statistically independent and cannot account for potential clustering of the data due to the within-subject repeated-measures design. To address this, since neighboring electrode contacts and repeated trials from the participant do not constitute independent samples, we used Generalized Estimating Equations (GEE) [26,27] to model relative theta power as a function of whether the participant was moving or not (see STAR Methods). In agreement with the results obtained from the theta power index distribution, we found that movement is indeed a significant factor in predicting relative theta power (P<0.001, Wald χ^2 =172.50; estimated means and 95% Wald confidence intervals are as follows: 0.70, [0.67, 0.73] for movement, and 0.30, [0.27, 0.33] for immobility).

Prevalence of Theta Oscillations

To further investigate how movement speed modulated theta, we quantified the prevalence of significant theta oscillations during fast versus slow movements using the BOSC method [28–30]. This method uses wavelets to provide a power estimate for the signal, and— accounting for the background 1/f dependency—can detect periods with significant oscillations at different frequencies that exceed thresholds for power and duration (see STAR Methods). This method was recently used by Watrous *et al.* [31] in a comparative study of theta oscillations between virtual navigation studies in humans and real world navigation studies in rodents. Therefore applying the BOSC method allowed for direct comparisons of our findings with previously published results.

For each participant and within each trial, data was separated into low and high speed movements using a median split on speed in that trial to obtain an equal amount of data within each condition (see STAR Methods). By utilizing the BOSC method [28,29], episodes with significant oscillations between 3–30 Hz (p-episodes, percent trial time in oscillatory episodes [29]; occurring for at least 3 cycles and above 95% chance level, Figure 4A) were calculated in frequency windows of 0.25 Hz (see STAR Methods). We found that in all 4 participants, there was a significant increase in theta oscillations during fast movements compared to slow movements (Figure 4B). This increase in the prevalence of theta, as quantified by p-episodes, was observed between 7–9.25Hz ($N_{trials \times channels}$=84,

p<0.05, clustered-based permutation test [32]; see STAR Methods) for the sighted participants and 6.5–8.75Hz in the congenitally blind participant ($N_{trials \times channels}$=28, p<0.05, clustered-based permutation test; note that these ranges were qualitatively similar using Wilcoxon rank-sum test). Interestingly, these theta episodes were transient and present ~10% of the time for the sighted group, while this percentage was ~30% in the congenitally blind participant (Figure 4B). Hence, we analyzed the data from the congenitally blind participant separately from the data from sighted participants, whose results were qualitatively similar to each other (Figure S3A). Moreover, we observed significant differences in p-episodes in higher frequencies (17.25–18.25Hz in sighted participants and 14.5–16.75Hz in the congenitally blind participant; clustered-based permutation test) (Figure 4B). This might suggest the presence of theta harmonics in our data, which have been reported to increase with movement speed in rats [33].

The differences in the prevalence of theta oscillations between the blind and sighted participants call for an assessment of sighted participants walking with their eyes closed. To address this, two of our participants (P1 and P5) performed the task while they were blindfolded and had their eyes closed. Although the overall speed was generally lower (median, [25th, 75th] = 0.28, [0.02, 0.60]), we found no qualitative differences in theta properties between the conditions with closed or open eyes (Figure S3B). This suggests that the congenitally blind participant may have developed a different strategy for navigating an environment that may not be readily available to sighted participants. We then asked whether there was a strategy that would result in higher prevalence of theta oscillations. To address this we asked a participant (P5) to walk back and forth on the same path while head-scanning left and right or looking at a fixed target on the wall. Here, we found that theta oscillations were more present during head-scanning behavior—quantified by larger angular speed of the participant's head (Figure 5; p-episode = 21.73±4.47% at peak frequency of 7.75Hz versus p-episode = 10.09±3.85% during walking while looking at a fixed target).

It is worth noting that there is an analog filter on the RNS® System, equivalent to a 1st order Butterworth with 3db attenuation at the cutoff frequencies (4–90Hz). Thus, it was necessary to test and validate our results to ensure that they were not an artifact of the filter. First, we used broadband data (0.1–8000 Hz) recorded from an independent group of participants (n=2), from a previous study by Suthana *et al.* [34], who were acutely implanted with depth electrodes for seizure monitoring during inpatient hospitalization (hereinafter referred to as depth subjects). Here, we confirmed that the BOSC method returned highly similar results, both in calculating power spectra and oscillation detection patterns, in the presence or absence of a mathematically implemented filter analogous to the one on the RNS® System (Figure S4A, b; see STAR Methods). Second, to further ensure that our results were not skewed by the analog filter on the RNS® System, we collected broadband data (0.1– 8000Hz) recorded from a single depth subject during movement. The participant was asked to walk slowly around his hospital room as we tracked his motion using Google's Project Tango tablet (see STAR Methods), which allowed us to perform the same analyses we used in participants with the RNS® System (Figure S4C). We used data from an electrode contact (macro-electrode; see STAR Methods) that fell within the MTL region (CA1) for further analysis. Due to the small variability in the walking speed—caused by the participant having to navigate in limited space around hospital equipment while tethered—we compared p-

episodes using the BOSC method during periods of movement versus immobility. Here too, our results showed a qualitatively similar percentage of time with significant theta oscillation during movement and demonstrated that higher frequency theta is more prevalent during movement versus immobility (Figure S4D), thus indicating that our oscillation detection method is robust.

Duration of Oscillatory Bouts

We next asked whether the increase in the prevalence of theta during fast versus slow movements was due to longer theta bouts or higher rates of occurrence. To address this, we computed the duration of oscillatory bouts by varying the threshold for the number of cycles required for significance (Figure 6A). We detected significant oscillatory episodes with at least one cycle, converted the total number of detected cycles in each bout to durations, and computed the average durations of these epochs in each frequency bin. Comparisons of the durations of theta bouts in fast and slow movements showed no significant difference in bout durations between the two conditions ($p > 0.05$ at any frequency; cluster-based permutation test) (Figure 6B). This suggests that more prevalent theta during fast movement potentially arises as a result of short theta bouts of similar lengths occurring more frequently during fast movements. We also observed that the average duration of theta bouts was higher in the congenitally blind participant (~570ms) compared to sighted participants (440ms) at the peak frequency (Figure 6B). It is worth mentioning that by comparing our results with those published by Watrous *et al.* [31] using the same method (Figure 2D), it is evident that our results from the blind participant are more similar to those observed in moving rodents. Moreover, our findings in sighted participants lie between rodent real-world navigation and human virtual navigation, further supporting the hypothesis that the observed theta oscillations in the current study are indeed movement related.

To test whether the movement speed (i.e. fast versus slow movement) can be decoded from the pattern of oscillations, we used a neural network machine-learning model—a commonly used method for classification, which is generally more flexible compared to other methods such as logistic regression [35](see STAR Methods). Here, power spectra—computed using wavelet analysis present in the BOSC method toolbox (Figure S5A; see STAR Methods)—were used as the input to our model in order to predict movement speed (Figure S5B). Data was divided into independent sets for training, cross-validation (to reduce overfitting), and testing. Receiver operating characteristic (ROC) plots and the area under these curves (AUC) —common measures of model performance in classification [36]—showed that the performance of our model was significantly better than chance in classifying fast from slow movement speeds (Figure S5C).

Discussion

We present a novel, innovative methodology for combining motion capture technology and continuous iEEG recordings, enabling access to the MTL in freely moving humans. To our knowledge, this study demonstrates the first quantification of theta oscillations during untethered ambulatory movement in humans. Our results show high frequency (~8Hz) theta oscillations occur during movement and exhibit a higher power compared to periods of

immobility. In addition, theta occurs in short bouts (~400ms) that are present more frequently during fast versus slow movement speeds and thus significantly differentiates the two.

Previous investigations of theta oscillations in primates have resulted in conflicting evidence regarding the presence and functionality of the theta rhythm compared to those in rodents [19,31,37,38]. These dissimilarities are thought to be, in part, attributed to the differences in the primary source of sensory information in these species—visual inputs in primates versus olfactory and somatosensory inputs in rodents. Nonetheless, the lack of feasibility in recording iEEG in freely moving primates (in contrast to rodents), has not previously allowed for unequivocal evaluation of theta oscillatory properties under similar conditions in these species. Our findings demonstrate that in humans, short, intermittent, theta bouts occur and are indeed movement related, but they are not as continuous as those found in rodents. Further, these bouts occur at a higher rate during fast movements. One possible explanation for this effect is that saccadic eye movements are the dominant source of sensory input as a means for exploration in primates [16,19,38]. Thus, if saccadic eye movements occur at a higher rate during faster locomotion, this could potentially lead to more frequent theta bouts. Whether theta bouts are elicited and phase-reset by saccades warrants further investigation.

Curiously, in our present results, significant theta oscillations occurred more often and more continuously in a single participant who is congenitally blind. This participant used a Hoover cane to traverse the environment, thereby possibly using somatosensory and path-integration inputs to a greater extent compared to other normally sighted participants. This may support the idea that the modality of sensory processing may be a critical factor relating theta oscillations to movement. Alternatively, it is argued that theta oscillations facilitate multisensory integration during active explorations and thus the differences between the blind participant and the sighted participants could have arisen as a result of how often exploration is required for navigation [16,38]. Given that somatosensory and path-integration cues—used by the blind participant and even rats—are more local compared to the distal visual cues, used by the sighted participants, they might be engaged more frequently during navigation. This might elucidate why theta in sighted humans is less continuous than theta in the blind participant and in rats and also explain why theta oscillations are present more often during fast movements compared to slow movements, and during head-scanning behavior.

While on average, the prevalence of theta oscillations were higher during fast versus slow movement, we observed differences in oscillation frequencies across regions and within individuals (Figure 4A). Thus, it is possible that there are subtle differences in oscillatory properties across MTL regions, which are not captured within our study. For example, in rodents, it has been shown that the frequency of theta oscillations decrease—albeit slightly —along the septotemporal axis of the hippocampus, and a similar decrease has been found in the dorsoventral axis of the entorhinal cortex [39–41]. Another recent study demonstrated that nonlinear dynamics of theta oscillations in rodents vary with movement speed and are modulated by hippocampal regions [33]. Lastly, theta oscillations are diminished in power and spatial selectivity is reduced in the ventral compared to dorsal hippocampus [40]. In humans, the dorsoventral distinction is thought to map onto the posterior-anterior

hippocampal axis [42]. Therefore, future larger sample studies will be necessary to characterize movement-related theta changes across MTL regions and the implications of these differences in the coordinating role of theta oscillations.

Recently, it has been argued that the human analogue of rodent theta oscillations exists in the lower (<4Hz) frequency range [37]. However, to our knowledge, the investigation of theta oscillations within the human MTL during real world ambulatory movement has been limited due to the restrictions of wired intracranial recording electrode technology and the electrical noise introduced in the recordings as a result of physical movement. Using wireless, chronically implanted electrodes, our results suggest there does, in fact, exist a higher frequency (~8Hz) theta oscillation in the human MTL associated with physical movement—a finding which was replicated in an independent study [22]. Furthermore, lower frequency theta (~4Hz) in humans has been observed in stationary virtual navigation and memory tasks [43–46]. However, due to the analog filter on the RNS® System, the current study cannot address the differences between the two types of theta oscillations, and future studies are needed to determine how low and high frequency theta dynamics interact during ambulatory movement compared to those in stationary behavioral tasks. While the high frequency theta presented in the current study varies significantly between different speeds of movement, its exact behavioral correlates remains to be examined. It must be borne in mind that the study participants were epilepsy patients with altered cognitive functions. Although the task employed in the current manuscript was not related to memory, and consequently all participants successfully performed the task, the relationship between theta oscillations and memory performance warrants further investigation in future experiments with memory demands.

Overall, the current study provides important insight into human MTL theta oscillations during ambulatory behavior and—by elucidating similarities as well as differences in theta dynamics—can bridge findings across species. We present a novel paradigm for the leveraging of FDA approved technology combined with motion tracking that allows for future investigation of neural oscillatory dynamics during real world behaviors in humans.

STAR Methods

CONTACT FOR REAGENT AND RESOURCE SHARING

Further information and requests should be directed to and will be fulfilled by the Lead Contact, Nanthia Suthana (nsuthana@mednet.ucla.edu).

EXPERIMENTAL MODEL AND SUBJECT DETAILS

Participants implanted with the RNS® System—Participants (Table S1) were 4 patients (three sighted and one congenitally blind) with pharmacoresistant epilepsy who had been previously implanted with the FDA approved NeuroPace RNS® System for treatment of epilepsy. The congenitally blind participant exhibited lifelong visual impairment with marginal light perception due to retinopathy of prematurity. Electrode placements were determined solely based on clinical treatment criteria. All participants volunteered for the study by providing informed consent according to a protocol approved by the UCLA

Medical Institutional Review Board (IRB). Neuropsychological scores for each individual were determined using methods previously described [34](Table S2).

Depth subjects—Participants were patients with pharmacoresistant epilepsy who were implanted with depth-electrodes for seizure monitoring. Electrophysiological data was recorded at 40KHz using ATLAS Data Acquisition system (Neuralynx, Bozeman, MT). A subset of this data was recorded and used in a previous study [34]. In addition, one depth subject was asked to walk back and forth in the hospital room (tethered) while holding Google's Project Tango tablet, which was equipped with motion tracking (https://get.google.com/tango/). The Paraview Tango Recorder application (https://blog.kitware.com/paraview-and-project-tango-loading-data/) was utilized to track their position. Data from a macro-electrode contact (1.5 mm diameter and surface area = 5.9 mm^2) located within the MTL region (CA1) (see Electrode localization methods) were used for further analysis.

METHOD DETAILS

Data acquisition—The FDA approved NeuroPace RNS® System (Figure 1A) is designed to be programmed to detect abnormal electrical activity in the brain and respond in a closed loop manner by delivering imperceptible levels of electrical stimulation intended to normalize brain activity before an individual experiences seizures. For the present study, a neurologist was present to configure stimulation to OFF and ON before and after the study and monitor for seizure activity. Each of the 4 participants in the study had two implanted depth electrode leads 1.27 mm in diameter each with 4 platinum-iridium electrode contacts, each with a surface area of 7.9 mm^2, 1.5 mm long with an electrode spacing of either 3.5 or 10 mm (Table S3). During the study, the RNS® Neurostimulator continuously monitored iEEG activity on four bipolar channels at 250 Hz with an analog filter equivalent to a 1st order Butterworth with 3db attenuation at the cutoff frequencies (4–90Hz). The neurostimulator communicates wirelessly with a Programmer and Remote Monitor using secure protocols. The Programmer is used to (1) retrieve data, including stored iEEG data, from the neurostimulator, (2) configure detection and stimulation, and (3) monitor iEEG activity and test stimulation settings in real-time. A programmable electromagnet was used to trigger iEEG storage in the RNS® Neurostimulator.

Electromagnet—A programmable electromagnet was designed to be placed on the participant's head over the RNS® Neurostimulator and trigger iEEG recordings by generating magnetic pulses. The magnetic pulses could be triggered either manually or automatically with programmable intervals of 30, 60, 90, 150, 180 and 240 seconds. Power was provided by rechargeable NICAD batteries. The electromagnet had a visible LED as well as an infrared LED, which were used both as visible indicators and event markers for synchronization of iEEG recordings with recorded video. The device accepts three commands: a hard reset command, which allows for either alteration of the timing or entering into the test mode; a clear command which is a soft reset in that any command other than reset is halted and all timing counters are cleared; and a start or stop command which starts the timing for the marker function.

Motion Tracking—Motion tracking was done using the Optitrack system (Natural Point, Inc.; http://optitrack.com/) with 8 ceiling mounted infrared high-resolution cameras that allow for sub-millimeter motion tracking. Removable reflective markers were used in conjunction with specialized software, Motive and Camera SDK, which allows for kinematic labeling. For the head, a rigid body object was constructed, from the reflective markers, for which center of mass (i.e. position) was tracked in addition to a quaternion describing rotational information that is translated to Euler angles to obtain yaw, pitch and roll with respect to the experimental room. This information was then used to obtain participants' movement trajectory and speed (Figure 1B, C, D). Further, another set of 4 ceiling mounted high-resolution Optitrack cameras were dedicated to record videos in the visible spectrum, which were then used for synchronization purposes (see below).

Synchronization of iEEG and motion capture data—When the electromagnet was activated, it triggered the storage of iEEG data by the RNS® System in preconfigured short durations (60 s), generated a "magnet marker" event in the iEEG data, as well as turned on a visible LED light, which was captured by the video cameras. The "magnet marker" events in the iEEG data were then aligned with the onset of the visible LED light events in our motion tracking system. This allowed us to synchronize the two data streams and combine the stored pieces of iEEG data into a long continuous recording.

Electrode Localization—Electrode localization was done using methods similar to those reported by Suthana *et al.* [34]. A high-resolution post-operative CT image was co-registered to a pre-operative whole brain and high-resolution MRIs for each participant (Figure 2B, Figure S6). We used the FSL FLIRT (FMRIB's Linear Registration Tool [47]) together with BrainLab stereotactic and localization software [48]. MTL regions (entorhinal, perirhinal, parahippocampal, hippocampal subfields CA23DG [CA2, 3, dentate gyrus], CA1, and subiculum) are anatomically determined by boundaries that are demarcated based on atlases correlating MRI visible landmarks with underlying cellular histology. To avoid human bias and perform hippocampal segmentation programmatically we used ASHS software [49].

Behavioral task—Participants performed a task in which they were directed to walk slow or fast following linear and circular paths in a 400 square foot room based on an auditory command. Each trial consisted of four different conditions: walking in a straight line or circle at slow or fast speeds, and the order in which these conditions were presented was randomized. This strategy yielded a relatively large range of movement speeds (Figure 1D). Furthermore, for each participant, the speed profile was similar across different trials (data not shown).

QUANTIFICATION AND STATISTICAL ANALYSIS

All analyses were done offline using custom code in MATLAB and SPSS.

Elimination of epileptic activity from iEEG—Data from putative epileptic epochs were discarded according to a method similar to procedures described recently [25] using functions found in MATLAB Signal Processing Toolbox. In brief, epileptic discharges were identified when either of the following conditions were satisfied: a) the envelope of the

unfiltered signal was 5 s.d. above the baseline; b) the envelope of the filtered signal (band-pass filtered in the 25–80Hz range followed by signal rectification) was 6 s.d. above the baseline (Figure S1). We excluded ~3% of the data from further analysis because of the presence of epileptic activity and this percentage was not significantly different between slow and fast movements (p = 0.6, Wilcoxon rank-sum test; Figure S1B). All of the iEEG traces used for analysis were also visually inspected for epileptic activity, before and after the automatic removal procedure.

Theta power index—For each trial, the theta power index was computed by subtracting the total power between 3–12Hz, henceforth referred to as theta power, during immobility from theta power during movement and normalizing the resulting value by the sum:

$$\theta \ power \ index \ = \ \frac{\theta_{movement} - \theta_{immobility}}{\theta_{movement} + \theta_{immobility}}$$

This measure varies between −1 and 1 with positive values indicating more theta power during movement.

Generalized Estimating Equations (GEE)—We used GEE, a class of regression marginal models, to examine the relationship between relative theta power and movement while accounting for potential clustering between the data points due to the within-subject repeated-measure design. Here, relative theta power was modeled using SPSS software (IBM Corporation, USA) with a movement condition (movement vs. immobility) as a predictor. We implemented the model with participant identity as a within-subject variable, exchangeable correlation matrix with robust covariance estimate, and using linear scale response (identity link function). Model statistics are reported as the estimated means and 95% Wald confidence intervals.

Detection of significant oscillations—BOSC algorithm was used [28–30], and episodes with significant oscillations between 3–12Hz (using 6th order wavelets and for bouts occurring for at least 3 cycles and above 95% chance level) were detected. Additionally, to examine the duration of theta bouts, the lower bound on the number of cycles for detection was allowed to vary.

Control analysis for oscillation detection—To evaluate the effect of the analog bandpass filter (1st order Butterworth 4–90Hz, 3db attenuation at cutoff frequencies) on the RNS® System on our results, we mathematically implemented this filter on data collected from a previous study [34] in participants with implanted depth electrodes. We first computed the power spectrum, using BOSC method, for randomly selected (N=100) 5-seconds-long iEEGs during trials (P_1). Power spectra were then computed for these iEEGs filtered using the abovementioned filter settings (P_2). A similarity index was computed between the two matrices (P_1 and P_2) using cosine distance defined as follows:

$$d_{ij} = \frac{p_{1i}p'_{2j}}{\sqrt{(p_{1i}p'_{1i})(p_{2j}p'_{2j})}}$$

A similarity index was then calculated while allowing for the frequency lower bound to vary (Figure S4A). The same procedure was done on the similarity index calculated between the matrices consisting of data points with significant oscillations (Figure S4B).

Extraction of theta from iEEG—Raw signal was bandpass filtered (between 3–12Hz) using an acausal 4th order Butterworth filter (Figure 2A). The phase and amplitude of theta was then computed from the filtered signal using Hilbert transform.

Statistics—Two-sided nonparametric Wilcoxon rank-sum test was utilized to assess the significant differences between linear variables. For each histogram, a kernel smoothing function was also computed for the probability density estimates. Values are expressed as median, [25th, 75th] or mean ± s.e.m when applicable. To control for family-wise error rates we used a method proposed by Maris and Oostenveld [32] that allows for multiple comparisons correction. In particular, when searching for frequency bins in which there were significant differences in oscillatory properties (p-episodes in Figure 4 and average duration of oscillatory bouts in Figure 6), the adjacent frequency bins cannot be assumed independent. Thus, the cluster-based permutation test performs 1000 permutations for an alpha level of 0.05 and finds clusters of significant data while accounting for multiple comparisons.

Classification of movement speed using machine learning—To classify behavior into fast and slow movement speeds (here referring to the top and bottom 30% of the running speeds respectively), we used a feed forward neural network with an input layer, a hidden layer consisting of 100 neurons and an output layer with a binary classifier (the corresponding speed categories). A tan-sigmoid function and a scaled conjugate gradient algorithm were used as a transfer function and back propagation algorithm respectively (Figure S5B). For each participant, the BOSC method was utilized to compute a power spectrum of the iEEG for each time point (Figure S5A). Data from all channels were concatenated (leaving a contiguous 15% of the total data out for the testing set to ensure independence). For the remaining data, 85% was used for training while the other 15% was used for cross validation. Receiver operating characteristic (ROC) plot and the area under that curve (AUC) were used to evaluate the performance of our model (Figure S5C).

DATA AND SOFTWARE AVAILABILITY

Data files, as well as the codes used in Matlab and SPSS, are available from the Lead Contact upon reasonable request.

Supplementary Material

Refer to Web version on PubMed Central for supplementary material.

Acknowledgments

References

1. Squire LR. Memory and the hippocampus: a synthesis from findings with rats, monkeys, and humans. Psychol Rev. 1992; 99:195–231. [PubMed: 1594723]

2. Squire LR, Stark CEL, Clark RE. THE MEDIAL TEMPORAL LOBE*. Annu Rev Neurosci. 2004; 27:279–306. [PubMed: 15217334]

3. Buzsáki G, Moser EI. Memory, navigation and theta rhythm in the hippocampal-entorhinal system. Nat Neurosci. 2013; 16:130–8. [PubMed: 23354386]

4. Jutras MJ, Buffalo EA. Oscillatory correlates of memory in non-human primates. Neuroimage. 2014; 85:694–701. [PubMed: 23867554]

5. Colgin LL. Rhythms of the hippocampal network. Nat Rev Neurosci. 2016; 17:239–249. [PubMed: 26961163]

6. Buzsaki, Gyorgy. Rhythms of the Brain. Oxford University Press; 2006.

7. Vanderwolf CH. Hippocampal electrical activity and voluntary movement in the rat. Electroencephalogr Clin Neurophysiol. 1969; 26:407–18. [PubMed: 4183562]

8. Robinson TE, Kramis RC, Vanderwolf CH. Two types of cerebral activation during active sleep: relations to behavior. Brain Res. 1977; 124:544–549. [PubMed: 192415]

9. Berry SD, Thompson RF. Prediction of learning rate from the hippocampal electroencephalogram. Science. 1978; 200:1298–300. [PubMed: 663612]

10. Klimesch W, Doppelmayr M, Russegger H, Pachinger T. Theta band power in the human scalp EEG and the encoding of new information. Neuroreport. 1996; 7:1235–1240. [PubMed: 8817539]

11. Seager MA, Johnson LD, Chabot ES, Asaka Y, Berry SD. Oscillatory brain states and learning: Impact of hippocampal theta-contingent training. Pnas. 2002; 99:1616–1620. [PubMed: 11818559]

12. Winson J. Loss of hippocampal theta rhythm results in spatial memory deficit in the rat. Science. 1978; 201:160–3. [PubMed: 663646]

13. Canolty RT, Knight RT. The functional role of cross-frequency coupling. Trends Cogn Sci. 2010; 14:506–15. [PubMed: 20932795]

14. Hasselmo ME. What is the function of hippocampal theta rhythm?–Linking behavioral data to phasic properties of field potential and unit recording data. Hippocampus. 2005; 15:936–49. [PubMed: 16158423]

15. Bland BH, Sainsbury RS, Creery BL. Anatomical correlates of rhythmical slow wave activity (theta) in the hippocampal formation of the cat. Brain Res. 1979; 161:199–209. [PubMed: 758971]

16. Ulanovsky N, Moss CF. Hippocampal cellular and network activity in freely moving echolocating bats. Nat Neurosci. 2007; 10:224–33. [PubMed: 17220886]

17. Yartsev MM, Ulanovsky N. Representation of three-dimensional space in the hippocampus of flying bats. Science. 2013; 340:367–72. [PubMed: 23599496]

18. Stewart M, Fox SE. Hippocampal theta activity in monkeys. 1991

19. Jutras MJ, Fries P, Buffalo EA. Oscillatory activity in the monkey hippocampus during visual exploration and memory formation. Proc Natl Acad Sci U S A. 2013; 110:13144–9. [PubMed: 23878251]

20. Lega BC, Jacobs J, Kahana M. Human hippocampal theta oscillations and the formation of episodic memories. Hippocampus. 2012; 22:748–761. [PubMed: 21538660]

21. Ekstrom AD, Caplan JB, Ho E, Shattuck K, Fried I, Kahana MJ. Human hippocampal theta activity during virtual navigation. Hippocampus. 2005; 15:881–9. [PubMed: 16114040]

22. Bohbot VD, Copara MS, Gotman J, Ekstrom AD. Low-frequency theta oscillations in the human hippocampus during real-world and virtual navigation. Nat Commun. 2017; 8:14415. [PubMed: 28195129]

23. Ravassard P, Kees A, Willers B, Ho D, Aharoni D, Cushman J, Aghajan ZM, Mehta MR, Aghajan MZ, Mehta MR. Multisensory control of hippocampal spatiotemporal selectivity. Science. 2013; 340:1342–6. [PubMed: 23641063]

24. Aghajan MZ, Acharya L, Moore JJ, Cushman JD, Vuong C, Mehta MR. Impaired spatial selectivity and intact phase precession in two-dimensional virtual reality. Nat Neurosci. 2014; 18:121–128. [PubMed: 25420065]

25. Gelinas JN, Khodagholy D, Thesen T, Devinsky O, Buzsáki G. Interictal epileptiform discharges induce hippocampal–cortical coupling in temporal lobe epilepsy. Nat Med. 2016; 22:641–648. [PubMed: 27111281]

26. Hardin, JW., Hardin, W, J. Encyclopedia of Statistics in Behavioral Science. Chichester, UK: John Wiley & Sons, Ltd; 2005. Generalized Estimating Equations (GEE).

27. Hubbard AE, Ahern J, Fleischer NL, Van der Laan M, Lippman SA, Jewell N, Bruckner T, Satariano WA. To GEE or Not to GEE. Epidemiology. 2010; 21:467–474. [PubMed: 20220526]

28. Hughes AM, Whitten TA, Caplan JB, Dickson CT. BOSC: a better oscillation detection method, extracts both sustained and transient rhythms from rat hippocampal recordings. Hippocampus. 2012; 22:1417–28. [PubMed: 21997899]

29. Caplan JB, Madsen JR, Raghavachari S, Kahana MJ. Distinct Patterns of Brain Oscillations Underlie Two Basic Parameters of Human Maze Learning. J Neurophysiol. 2001; 86

30. Whitten TA, Hughes AM, Dickson CT, Caplan JB. A better oscillation detection method robustly extracts EEG rhythms across brain state changes: the human alpha rhythm as a test case. Neuroimage. 2011; 54:860–74. [PubMed: 20807577]

31. Watrous AJ, Lee DJ, Izadi A, Gurkoff GG, Shahlaie K, Ekstrom AD. A comparative study of human and rat hippocampal low-frequency oscillations during spatial navigation. Hippocampus. 2013; 23:656–61. [PubMed: 23520039]

32. Maris E, Oostenveld R. Nonparametric statistical testing of EEG- and MEG-data. J Neurosci Methods. 2007; 164:177–190. [PubMed: 17517438]

33. Sheremet A, Burke SN, Maurer AP. Movement Enhances the Nonlinearity of Hippocampal Theta. J Neurosci. 2016; 36

34. Suthana NA, Parikshak NN, Ekstrom AD, Ison MJ, Knowlton BJ, Bookheimer SY, Fried I. Specific responses of human hippocampal neurons are associated with better memory. Proc Natl Acad Sci. 2015; 112:10503–10508. [PubMed: 26240357]

35. Dreiseitl S, Ohno-Machado L. Logistic regression and artificial neural network classification models: A methodology review. J Biomed Inform. 2002; 35:352–359. [PubMed: 12968784]

36. Jin, Huang, Ling, CX. Using AUC and accuracy in evaluating learning algorithms. IEEE Trans Knowl Data Eng. 2005; 17:299–310.

37. Jacobs J, Scoville W, Milner B, Berry S, Thompson R, Moser MBM, Moser E, O'Keefe J, Nadel L, Eichenbaum H, et al. Hippocampal theta oscillations are slower in humans than in rodents: implications for models of spatial navigation and memory. Philos Trans R Soc Lond B Biol Sci. 2014; 369:20130304. [PubMed: 24366145]

38. Geva-Sagiv M, Las L, Yovel Y, Ulanovsky N. Spatial cognition in bats and rats: from sensory acquisition to multiscale maps and navigation. Nat Rev Neurosci. 2015; 16:94–108. [PubMed: 25601780]

39. Hasselmo ME, Giocomo LM, Zilli EA. Grid cell firing may arise from interference of theta frequency membrane potential oscillations in single neurons. Hippocampus. 2007; 17:1252–1271. [PubMed: 17924530]

40. Royer S, Sirota A, Patel J, Buzsaki G. Distinct Representations and Theta Dynamics in Dorsal and Ventral Hippocampus. J Neurosci. 2010; 30:1777–1787. [PubMed: 20130187]

41. Patel J, Fujisawa S, Ber??nyi A, Royer S, Buzs??ki G. Traveling Theta Waves along the Entire Septotemporal Axis of the Hippocampus. Neuron. 2012; 75:410–417. [PubMed: 22884325]

42. Strange BA, Witter MP, Lein ES, Moser EI. Functional organization of the hippocampal longitudinal axis. Nat Rev Neurosci. 2014; 15:655–669. [PubMed: 25234264]

43. Kahana MJ, Seelig D, Madsen JR. Theta returns. Curr Opin Neurobiol. 2001; 11:739–744. [PubMed: 11741027]

44. Jacobs J, Kahana MJ. Direct brain recordings fuel advances in cognitive electrophysiology. Trends Cogn Sci. 2010; 14:162–171. [PubMed: 20189441]

45. Buzsáki G. Theta rhythm of navigation: link between path integration and landmark navigation, episodic and semantic memory. Hippocampus. 2005; 15:827–40. [PubMed: 16149082]

46. Rutishauser U, Ross IB, Mamelak AN, Schuman EM. Human memory strength is predicted by theta-frequency phase-locking of single neurons. Nature. 2010; 464:903–907. [PubMed: 20336071]

47. Jenkinson M, Smith S. A global optimisation method for robust affine registration of brain images. Med Image Anal. 2001; 5:143–156. [PubMed: 11516708]

48. Gumprecht HK, Widenka DC, Lumenta CB. BrainLab VectorVision Neuronavigation System: technology and clinical experiences in 131 cases. Neurosurgery. 1999; 44:97–104. 5. [PubMed: 9894969]

49. Yushkevich PA, Wang H, Pluta J, Das SR, Craige C, Avants BB, Weiner MW, Mueller S. Nearly automatic segmentation of hippocampal subfields in in vivo focal T2-weighted MRI. Neuroimage. 2010; 53:1208–24. [PubMed: 20600984]

Highlights

- Movement-related 8Hz theta oscillations occur in the human medial temporal lobe.

- Theta occurs in short bouts that are more prevalent during fast vs. slow movements.

- The duration and prevalence of theta is higher in a congenitally blind participant.

- Combined motion capture and iEEG allows for future studies of ambulatory behavior.
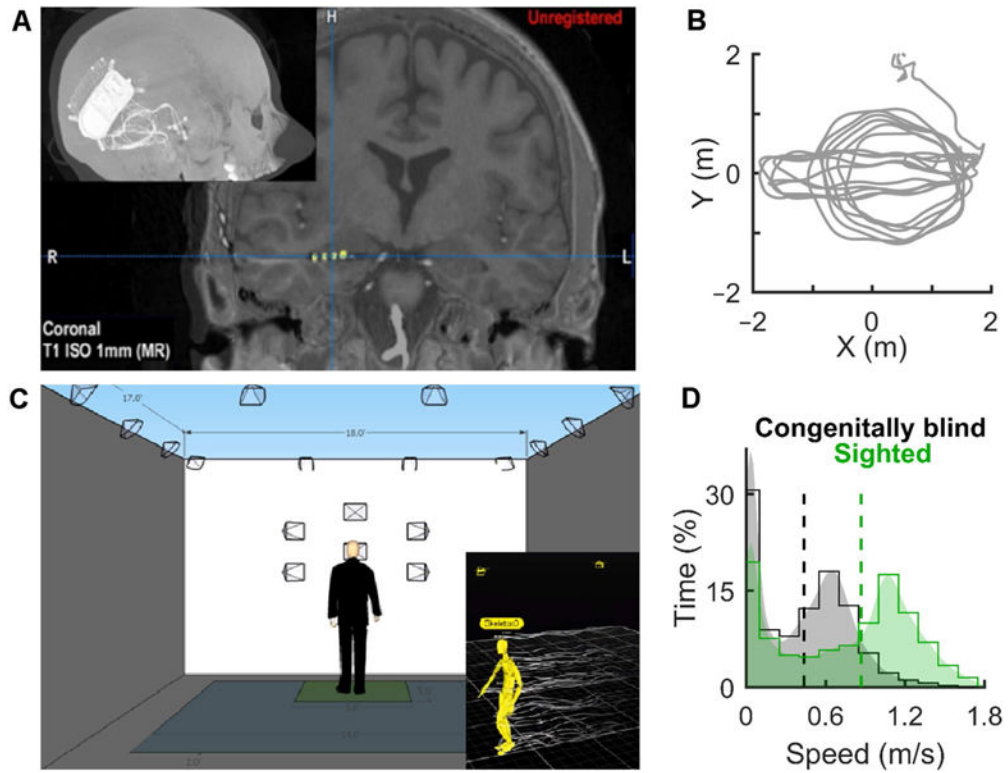
Figure 1. Simultaneous motion tracking and iEEG recording within the human MTL
(A) Example post-operative CT of a participant with an implanted electrode in the right hippocampus (top left) along with a coronal view of a high-resolution MRI overlaid with co-registered electrodes (shown in yellow). **(B)** Sample trajectory of a participant during one complete trial consisting of linear and circular movements. **(C)** Schematic of the setup of cameras used for motion capture (see STAR Methods). Inset: Real time motion tracking of an example participant. **(D)** Movement speed distribution of all sighted participants (green; median, $[25^{th}, 75^{th}] = 0.87$, $[0.20, 1.14]$ m/s, $N_{trials \times channels} = 84$) and congenitally blind participant (black; median, $[25^{th}, 75^{th}] = 0.44$, $[0.05, 0.68]$ m/s, $N_{trials \times channels} = 28$; dashed vertical lines indicate median value; shaded areas correspond to kernel smoothing function estimates of the distributions). See also Tables S1, S2, and Movie S1.
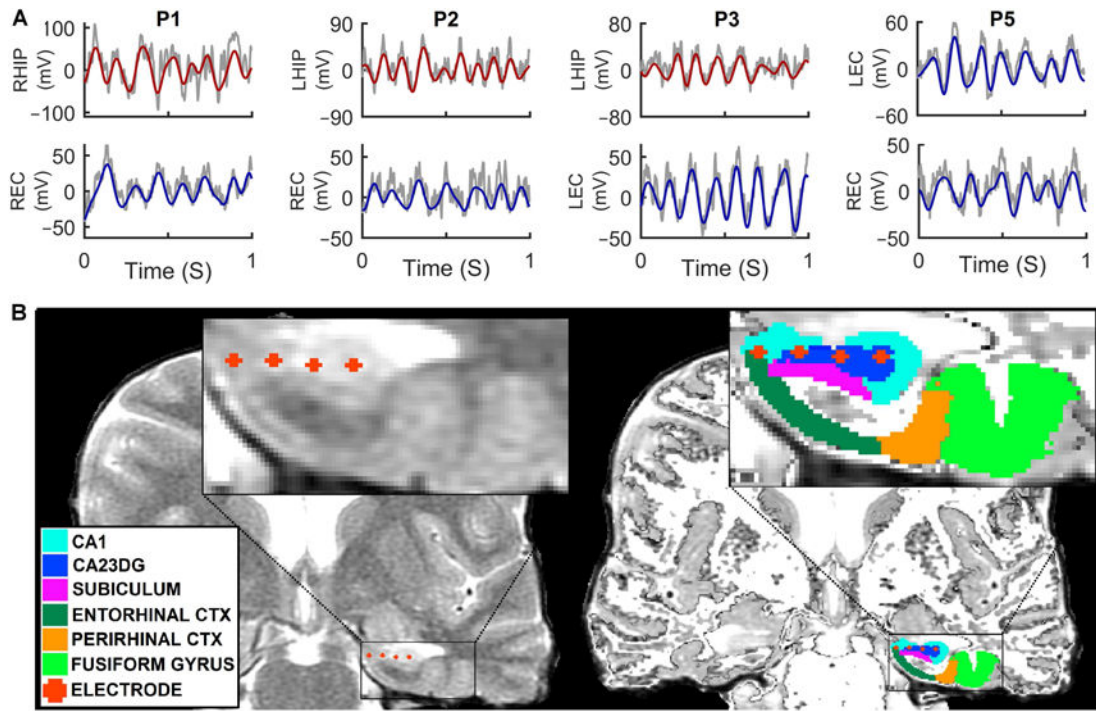
Figure 2. Example theta oscillations in the human MTL

(A) Example one-second-long raw iEEG traces (gray) from the MTL of all study participants overlaid with filtered (3–12Hz) theta oscillations (hippocampal and entorhinal theta shown in red and blue respectively). Participant P3 is congenitally blind. Note that on average, the duration of theta bouts are shorter than 1s as demonstrated in this figure (for a detailed characterization, see Figure 4). **(B)** Left) Sample electrode locations from a participant (P2) overlaid onto coronal pre-operative high-resolution MRI. Right) Automated MTL subregion segmentation (note that different colors correspond to different areas) demonstrating electrode locations in an example participant. White areas correspond to white matter. See also Figures S1, S6, Table S3, and Movies S2, S3.
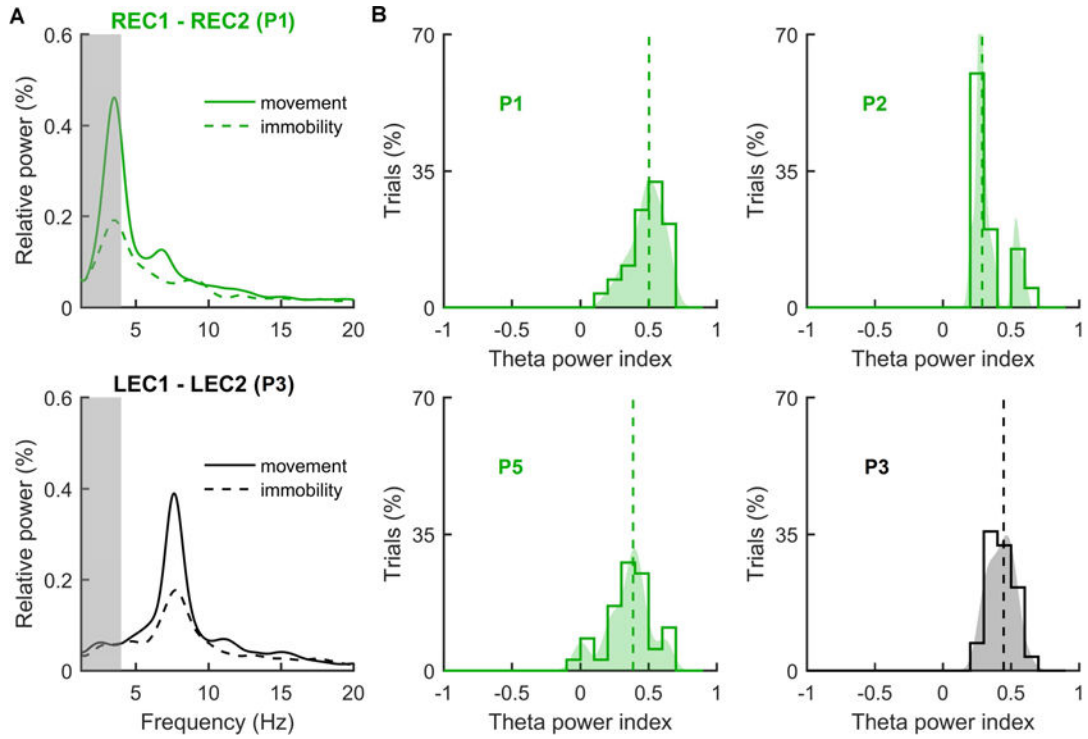
Figure 3. Theta power during movement versus periods of immobility
(A) Example (normalized) power spectra from a sighted participant (P1, top, green) and the congenitally blind participant (P3, bottom, black) displaying more theta power during movement (solid lines) compared to immobility (dashed lines). The power spectrum for each trial was normalized by the average power in that trial, during movement and immobility, over the frequency range 3–12Hz. Values below 4 Hz (lower range of the analog bandpass filter) are marked with shaded gray areas. Channel names are labeled clinically and for a detailed description, see Table S3. The recordings were bipolar using adjacent electrodes 1–2 and 3–4 (e.g. REC1-REC2 is one iEEG channel). The two adjacent electrodes in iEEG channel REC1-REC2 in participant P1 were located in the right entorhinal cortex (REC1) and right perirhinal cortex (REC2). The two adjacent electrodes in iEEG channel LEC1-LEC2 in participant P3 were located in the left entorhinal cortex (LEC1) and left perirhinal cortex (LEC2). **(B)** Theta power index was significantly positive for all participants as shown above, thus indicating higher theta power during movement (sighted participants (green); P1: 0.50, [0.43, 0.57], p=3.79×10^{-16}; P2: 0.29, [0.27, 0.36], p=8.86×10^{-5}; P5: 0.39, [0.24, 0.43], p=2.36×10^{-7}; congenitally blind participant (black); P3: 0.45, [0.35, 0.50], p=3.79×10^{-6}; Wilcoxon signed rank test was used because not all of the distributions passed the Lilliefors test of normality). Shaded area corresponds to kernel smoothing function estimate of the distribution and the dashed line indicates the median value. See also Figure S2, Table S3.
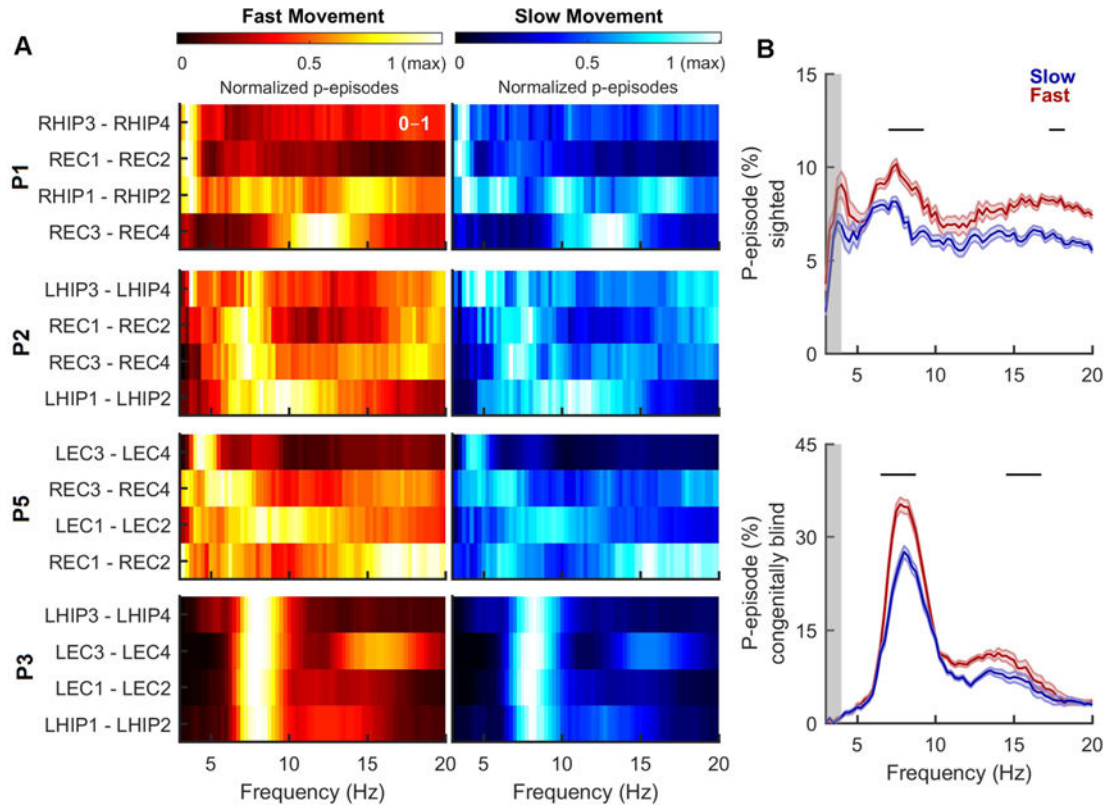
Figure 4. Significant increase in the prevalence of high-frequency theta oscillations during fast compared to slow movement

(A) Colormap shows percentage of time with significant oscillations (p-episode) in the frequency range indicated on the x axis averaged across trials for each clinically labeled channel in the left and right entorhinal cortex (LEC, REC) and left and right hippocampus (LHIP and RHIP) from all participants (electrode 1: most distal, electrode 4: most proximal; The electrodes were implanted orthogonal to the surface of the brain, thus distal and proximal correspond to deeper and shallower contacts respectively). Channel names are labeled clinically; for a detailed description of the localizations, see Table S3. Data are normalized by the maximum value for each channel, within each condition, for visibility purposes (range: 0–1). Brighter colors indicate larger values as demonstrated by the colorbars. Throughout this figure, red shades and blue shades correspond to fast and slow movements respectively. Also, note that for each participant, channels are sorted based on the frequency with maximum prevalence during fast movements, i.e. the frequency with maximum p-episodes in each channel increases from top to bottom rows. **Left:** Shown are normalized p-episodes during fast movement. Lighter shades indicate higher values here and throughout figures (N_{trials} for participants P1, P2, P5 and P3 (congenitally blind) were 7, 5, 9 and 7 respectively). **Right:** Same as (**left**) but during movement at slow speeds. **(B)** Percentage of time with significant oscillations (across all trials and channels; shown are mean ± s.e.m) during fast movements (red) versus slow movements (blue) in 3 sighted participants (top, $N_{trials \times channels}=84$) and 1 congenitally blind participant (bottom, $N_{trials \times channels}=28$). Black horizontal lines indicate regions with significant difference in p-episodes between fast and slow movement conditions (p < 0.05, clustered-based permutation

test). Values below 4 Hz (lower range of the analog bandpass filter) are marked with shaded gray areas. See also Figures S3, S4, S5, and Table S3.
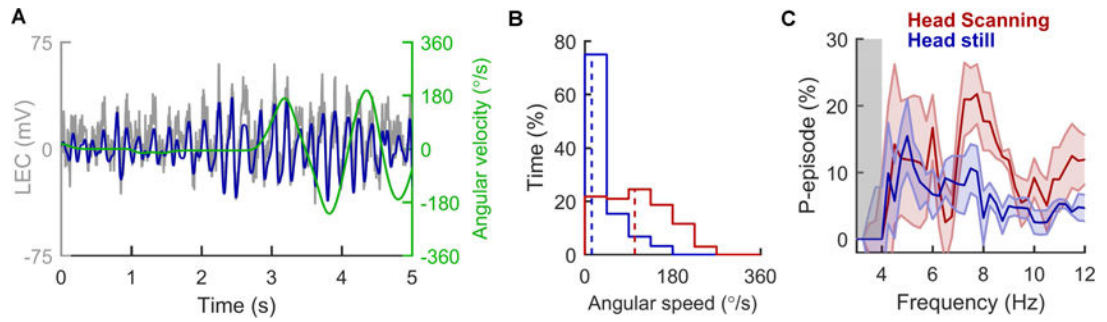
Figure 5. Theta oscillations are more prevalent during head-scanning behavior
(A) Example raw iEEG trace (gray) from a participant (P5) overlaid with filtered (3–12Hz) theta oscillations (blue) while he walked down the same path with and without head-scanning left and right. Green trace demonstrates the angular velocity of the head. **(B)** The participant was able to perform the task and periods with head-scanning behavior (red) manifested higher head angular speed (dashed line denotes the median value). **(C)** Head-scanning behavior resulted in higher presence of theta oscillations (red curve: p-episode = 21.73±4.47% at peak frequency of 7.75Hz) compared to periods when the participant walked looking at a fixed target (blue curve; p-episode = 10.09±3.85% at 7.75Hz). Shown are the mean ± s.e.m. values. Values below 4 Hz (lower range of the analog bandpass filter) are marked with shaded gray areas.
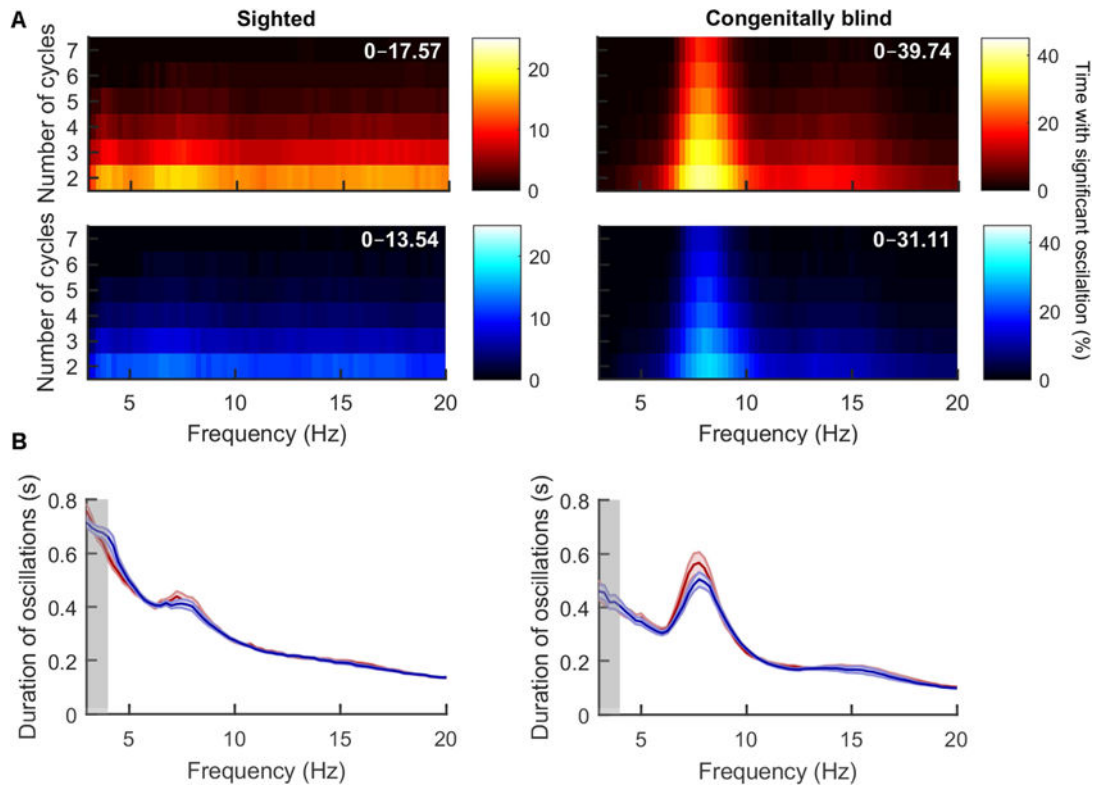
Figure 6. Duration of theta bouts is similar during fast and slow movements
(A) Colormaps indicate percentage of time with significant oscillations (p-episodes) in each frequency (averaged across trials, channels and participants) assuming varying number of minimum cycles for detection (y-axis). Red and blue color schemes correspond to fast and slow movements respectively, here and throughout the figure. Number at the top right corner indicates range. **(B)** Duration of significant oscillations at each frequency is shown as mean ± s.e.m across all trials and channels. There was no significant difference between the duration of the bouts between fast (red) and slow (blue) movements. However, note that in the congenitally blind participant (right), the duration of theta bouts (0.57s at peak frequency of 7.75Hz) were longer than those in the sighted participants (left, 0.44s at peak frequency of 7.25Hz). Values below 4 Hz (lower range of the analog bandpass filter) are marked with shaded gray areas.